ISSN 0031-918X, Physics of Metals and Metallography, 2022, Vol. 123, No. 1, pp. 92–98. © Pleiades Publishing, Ltd., 2022.
Russian Text © The Author(s), 2022, published in Fizika Metallov i Metallovedenie, 2022, Vol. 123, No. 1, pp. 101–108.

STRENGTH AND PLASTICITY

Effect of the Quenching Temperature on the Creep Resistance of 9% Cr–1% W–1% Mo–V–Nb Martensite Steel

A. E. Fedoseeva[a], *, I. S. Nikitin[a], and R. O. Kaibyshev[a]

[a] *Belgorod National Research University, Belgorod, 308015 Russia*

**e-mail: fedoseeva@bsu.edu.ru*

Received July 2, 2021; revised September 16, 2021; accepted September 20, 2021

Abstract—The creep resistance of the 9% Cr–1% W–1% Mo steel subjected to quenching from the temperatures of 1050 and 1150°C, cooling in the air, and further tempering at a temperature of 750°C for 3 h has been studied at a temperature of 650°C and applied stresses of 160, 140, and 120 MPa. An increase in the quenching temperature from 1050 to 1150°C leads to a growth in the average size of prior austenite grains from 25 to 93 μm due to the dissolution of MX carbonitride particles enriched in niobium under exposure in the austenite region. An increase in the size of the prior austenite grains is accompanied by a decrease in the average size of blocks and martensite laths by 17 and 43%, respectively. Moreover, an increased temperature of heating for quenching provides favorable conditions (fraction of boundaries, density of dislocations, and content of doping elements in a solid solution) for the precipitation of carbide $M_{23}C_6$ and carbonitride MX particles of smaller size under tempering. The improvement of structural hardening due to a decreased size of blocks and martensite laths and dispersion hardening due to nanosized VX particles has a positive effect on the creep resistance by decreasing the minimum creep rate and the duration of the transient creep stage to increase the time until rupture by several times.

Keywords: creep-resistant steel of martensite class, heat treatment, creep, microstructure, particles of secondary phases

DOI: 10.1134/S0031918X22010033

INTRODUCTION

At present, the development of thermoenergetic field is aimed at improving the performance efficiency of thermal power plants via the transition to ultrasupercritical steam parameters by increasing the steam temperature to 600–620°C and pressure to 25–30 MPa [1–3]. This is attained by passing to the use of heat-resistant steels of a new generation. Several high-chromium steels certified for application in thermoenergetics, such as steels P91, P911, and P92, were developed abroad as a material for the manufacture of the high-temperature circuits of boilers and main steam pipelines [1–3]. The broadest application is found for steels P911 (chemical composition, wt %: 0.1C–0.05N–9Cr–1W–1Mo–0.24V–0.07Nb–0.003B) and P92 (chemical composition, wt %: 0.1C–0.05N–9Cr–1.8W–0.6Mo–0.24V–0.07Nb–0.003B), which are suitable for prolonged operation at temperatures of up to 600°C and short-life service up to 620°C [1].

The structure of these steels represents tempered martensite lath structure formed by means of heat treatment composed of quenching in the air and medium-temperature tempering [1, 4, 5]. A complex hierarchical structure of tempered martensite lath structure represents prior austenite grains (PAGs) divided into packets [1–5]. The boundaries of these structural elements are high-angle ones [1–5]. The packets are divided by special boundaries or low-angle boundaries with a misorientation angle of 10.54° into blocks composed of martensite laths [1–5]. The boundaries of martensite laths are characterized by a misorientation angle from 1° to 2° [1–5]. A high creep resistance of these steels is provided by the superposition of all the four hardening mechanisms: (a) solid solution hardening, for which Cr, W, and Mo are responsible, (b) dislocation hardening, (c) substructural hardening by low-angle boundaries of martensite laths, and (d) dispersion hardening by carbonitride MX particles MX (where M is V, Nb, and X is C and/or N), which are uniformly distributed over the matrix bulk, chromium enriched carbides $M_{23}C_6$, and Laves phase intermetallides $Fe_2(W,Mo)$ precipitating on the boundaries of prior austenite grains, packets, blocks, and martensite laths [6]. The most important mechanism of hardening in high-chromium steels is dispersion hardening due to carbonitrides MX. These nanosized carbonitrides serve as hindrances for the motion of dislocations, thereby providing a low creep rate and a stable structure of tempered martensite lath structure at high temperatures [7–9]. The formation of two types of carbonitrides with a chemical composition of V(C,N) and

Nb(C,N) provides the stability of these particles in the process of creep at temperatures of up to 650°C [9].

The contributions from these hardening mechanisms to the ultimate yield strength and creep resistance can be influenced by changing the structure and distribution of the particles of secondary phases in tempered martensite lath structure due to variations in the regimes of heat treatment. The temperature of heating for quenching has an effect not only on the size of prior austenite grains, but also on the size of packets, blocks, carbides $M_{23}C_6$, and the predominant type of boundaries on which these carbides precipitate [10–13]. In the paper [10], it is pointed out that the long-term creep strength of steels with different doping, but with similar PAG sizes, will be the same, despite essential distinctions in short-term creep tests. In this case, the optimal size of PAGs is 50 μm [11]. The effect produced by the size of PAGs on the creep resistance of high-chromium steels remains unclear in many respects, taking into account a limited number of studies [10–13]. In these studies, steels with a different content of doping elements were compared to give no possibility to distinguish the effects of doping from the effects of thermal treatment. The objective of this study was to establish the effect of the quenching temperature on the creep resistance of 9% Cr–1% W–1% Mo–V–Nb steel at a temperature of 650°C.

METHOD OF STUDIES

9% Cr steel—hereinafter, steel P911—melted in a high-frequency induction furnace in OAO NPO TsNIITMASh (Moscow, Russia) has the chemical composition (wt %) 0.12% C–8.7% Cr–1% Mo–0.9% W–0.2% V–0.07% Nb–0.1% Si–0.4% Mn–0.2% Ni–0.05% N–0.003% B–0.02% Al. Forged workpieces were subjected to two regimes of heat treatment (conventional and modified), which consisted in quenching with further medium-temperature tempering. The conventional thermal treatment of steel P911 consisted in quenching from 1050°C with exposure for 30 min, cooling in the air, and further tempering at 750°C for 3 h with cooling in the air. The modified heat treatment of this steel was different only in that the temperature of heating for quenching was 1150°C.

The tests for creep until rupture were performed at a temperature of 650°C and applied stresses of 160, 140, and 120 MPa on flat specimens with the gauge length of 25 mm and a cross section of 7×3 mm^2 on an ATS2330 level-type testing machine. The size of prior austenite grains in the studied steel was estimated on an Olympus GX71 optical microscope (OM). The microstructure was revealed by chemical etching in a solution with the following composition: HF, 1%; HNO_3, 2%; H_2O, 97%.

Transmission electron microscopy (TEM) on a JEM JEOL-2100 microscope equipped with an INCA energy dispersive attachment and scanning electron microscopy (SEM) on a Quanta 600 3D microscope equipped with an attachment for electron backscatter (EBSD) analysis were used to estimate the sizes of packets and martensite laths, the density of dislocations, and the type, morphology, and size of secondary particles. EBSD-images were taken from 200×100 μm^2 surface areas with a step of 0.1 μm. Foils for TEM and EBSD analysis were prepared in a 10% perchloric acid solution in acetic acid at a voltage of 21–23 V on a special Struers TENUPOL-5 setup. Carbon replicas for TEM are obtained with the use of a Quorum Q 150R universal vacuum cart. The size of blocks and laths was determined by the random linear intercept method with the consideration for all the visible boundaries/(sub)boundaries. The density of free dislocations inside laths/subgrains was estimated from the amount of the points of dislocation intersections with the foil surface with the use of transmission electron microscopy and the Kernel coefficient from EBSD-images as $\rho = 2\varphi/xb$, where φ is the average Kernel coefficient as the mean lattice distortion around each scanning point for the first coordination sphere, x is the scanning step, and b is the Burgers vector [14]. The type of particles was determined by the complex method from the local chemical composition and TEM electron microdiffraction pictures of carbon replicas. The volumetric content of secondary phases was estimated by the Thermo-Calc software. The methods are described in more detail in the previous papers [6, 7, 13, 15].

STUDY RESULTS AND THEIR DISCUSSION

Effect of the Quenching Temperature on the Size of Initial Austenite Grains and the Secondary Phases

The optical metallography of steel P911 is shown in Fig. 1. An increase in the quenching temperature from 1050 to 1150°C leads to an essential growth in the average size of prior austenite grains from 25 ± 5 to 93 ± 5 μm, respectively (Fig. 1). An increase in the size of prior austenite grains is provoked by the dissolution of carbonitrides MX under exposure in the austenite region. The simulation of phase composition by the Thermo-Calc software has shown that carbonitrides MX enriched in vanadium and niobium persist at both quenching temperatures of 1050 and 1150°C. Let us point out that the chemical composition of the MX phase at the quenching temperatures of 1050 and 1150°C is essentially different. At $T = 1050$°C, carbonitride (Nb,V)X contains 40 wt % Nb–39% V–15% N–4% Cr–2% C. At $T = 1150$°C, carbonitride NbX contains 80 wt % Nb–4% V–8% N–3% Cr–5% C. The volumetric content of carbonitrides NbX is 0.11% at a quenching temperature of 1050°C and, when the quenching temperature grows to 1150°C, decreases to 0.024% to become nearly four times lower than at a lower quenching temperature. After quench-

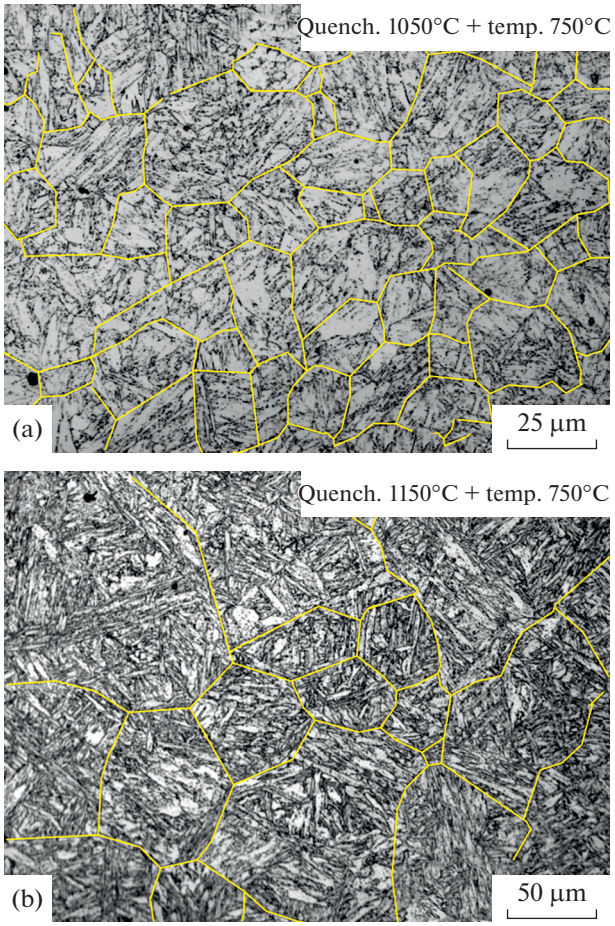

Fig. 1. OM images of the microstructure of steel P911 after quenching from (a) 1050 and (b) 1150°C with further tempering at 750°C with AIG boundaries shown in color.

ing, 0.16 wt % of V and 0.011 wt % of Nb at 1050°C and 0.20 wt % of V and 0.024 wt % of Nb at 1150°C persist in the solid solution to take part in the formation of carbonitride MX particles under further tempering at 750°C.

Effect of the Size of Initial Austenite Grains on the Creep Resistance

The dependence of the time until rupture on the applied stress for steel P911 after heat treatment by two regimes is shown in Fig. 2. It can be seen that an increase in the quenching temperature leads to an essential increment of 10, 5, and 4 times in the time until destruction at applied stresses of 160, 140, and 120 MPa, respectively (Fig. 2). The time until rupture τ_r can be expressed through the applied stress σ by the following equation [10]:

$$\tau_r = A\sigma^{-m}, \quad (1)$$

where A is a constant and m is the stress constant. The stress constants are 11 and 6 for quenching at temperatures of 1050 and 1150°C, respectively (Fig. 2). Such values correspond to dislocation creep controlled by the low-temperature climb of dislocations, whose rate is controlled by pipe diffusion [2, 10]. Let us point out that an increment in the time until rupture becomes smaller with a decrease in the applied stresses until complete disappearance (Fig. 2).

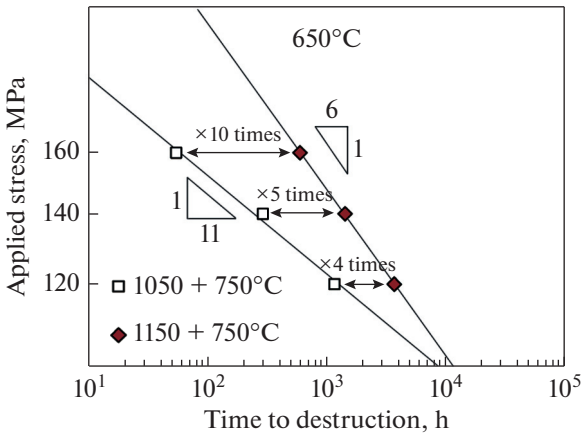

Fig. 2. Time until rupture versus applied stress at a temperature of 650°C for steel P911 subjected to different regimes of thermal treatment.

The dependences of the creep rate on the time and strain of deformation at a temperature of 650°C and applied stresses of 160, 140, and 120 MPa are shown in Fig. 3. Let us point out that the behaviour of creep curves is similar for both quenching temperatures. For each state, it is possible to distinguish three creep stages: the transient creep stage, at which the creep rate decreases to a minimum with an increase in the time and strain of deformation; the attainment of a minimum creep rate; and the accelerated creep stage, at which the deformation rate grows with an increase in the time and strain of deformation after attaining a minimum creep rate up to destruction (Fig. 3).

At all the applied stresses, steel P911 subjected to quenching from 1150°C with further tempering at 750°C demonstrates an increase in the time of the transient creep stage and a decrease in the minimum deformation rate by 1–2 orders of magnitude as compared to the conventional heat treatment (Fig. 3). It is just this factor that is responsible for a longer time until rupture under the same creep conditions (Fig. 2). However, this difference is reduced with a decrease in the applied stresses. Thus, at an applied stress of 160 MPa, an increase in the time of the transient creep stage is 10 times, being only 4 times at 120 MPa (Figs. 3a–3c). Moreover, the time required to attain the steady-state stage for the steel quenched from 1150°C exceeds the time until rupture for the steel quenched from 1050°C at all the applied stresses (Figs. 3a–3c).

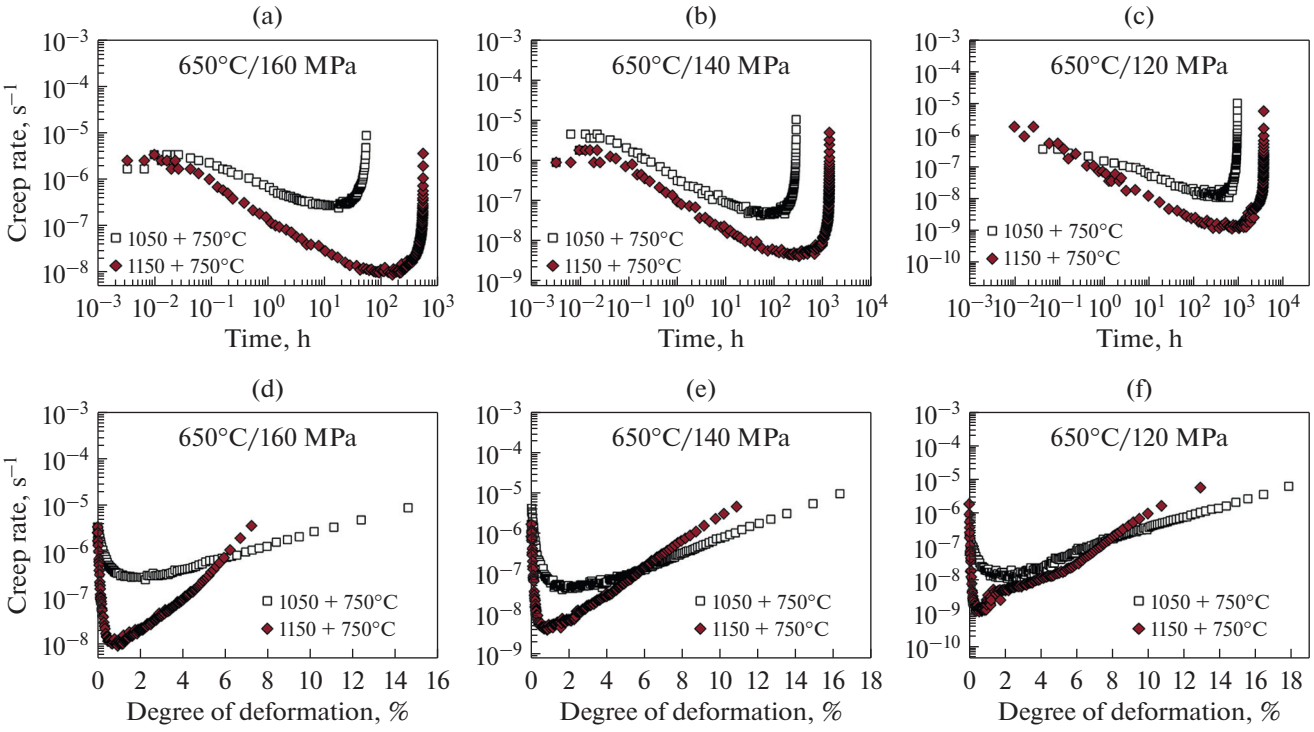

Fig. 3. Creep rate versus (a–c) time and (d–f) degree of deformation at a temperature of 650°C and applied stresses of (a, d) 160, (b, e) 140, and (c, f) 120 MPa for P911 steel after different regimes of thermal treatment.

At all the applied stresses, steel P911 subjected to quenching from 1050°C has a degree of deformation until rupture at a level of 15–18% (Figs. 3d–3f). At an applied stress of 160 MPa, the strain in steel P911 until rupture after quenching from 1150°C is two times lower than after quenching from 1050°C (Fig. 3d) and, however, this difference is reduced to 30% with a decrease in the applied stresses (Figs. 3e and 3f). Let us point out that the quenching temperature has a little effect on the degree of deformation of the transient creep stage (Figs. 3d–3f). At all the applied stresses, the strain, at which a minimum deformation rate is attained, is close to 1% for both states of steel P911 (Fig. 3).

Hence, an increase in the time until rupture in steel P911 subjected to quenching from 1150°C correlates with the more prolonged transient creep stage and a decrease in the minimum deformation rate and may be caused by both the structure formed after tempering and the microstructural transformations occurring at the transient stage of creep [13].

Some Microstructural Aspects of High Creep Resistance in the Steel with a Large Size of Initial Austenite Grains

To clarify the reasons for a higher strength of steel P911 with a larger size of PAGs, some detailed microstructural studies were performed by the transmission electron microscopy of foils and carbon replicas with the EBSD analysis after different heat treatments. The microstructure of steel P911 after quenching from 1050 and 1150°C with further tempering at 750°C is illustrated in Fig. 4. The structural parameters of steel P911 after different regimes of heat treatments are summarized in Table 1.

TEM of thin foils together with EBSD analysis has revealed that both thermal treatments lead to the formation of a tempered martensit lath structure. An increase in the quenching temperature from 1050 to 1150°C leads to a decrease of 17 and 43% in the size of a block and the width of martensite laths, respectively, despite a growth in the size of prior austenite grains (Table 1). The ratio between the size of a block and the width of martensite laths grows from 4.8 to 7 with an increase in the quenching temperature (Table 1). Let us point out that the density of dislocation estimated by TEM and EBSD analysis (using the Kernel coefficient) is independent of the quenching temperature and has the same order (Table 1), though the width of martensite laths and the density of dislocations in 9–12% Cr steels usually have a reciprocal dependence [6, 16].

After both types of heat treatments, spherical $M_{23}C_6$ carbide particles were revealed on the boundaries of PAGS, packets, blocks, and martensite laths. An increase in the quenching temperature from 1050 to 1150°C leads to a decrease in the size of $M_{23}C_6$ carbide particles from 97 to 83 nm with a simultaneous

Table 1. Structural parameters of steel P911 after different regimes of thermal treatment

Parameters	T_{quench}	
	1050°C	1150°C
Size of PAGs, μm	25 ± 5	93 ± 5
Block size, μm	2.6 ± 0.1	2.2 ± 0.1
Width of strips, μm	0.54 ± 0.05	0.31 ± 0.05
Density of dislocations (TEM), $\times 10^{14}$ m^{-2}	1.8 ± 0.1	2.1 ± 0.1
Density of dislocations (EBSD analysis), $\times 10^{14}$ m^{-2}	8.0 ± 0.1	7.6 ± 0.1
$M_{23}C_6$ size, nm	97 ± 5	83 ± 5
Density of particles along boundaries, μm^{-1}	1.44 ± 0.2	1.03 ± 0.2
NbX size, nm	41 ± 5	23 ± 5
VX size, nm	30 ± 5	18 ± 5
Volumetric content of VX, %	0.29	0.30

decrease in their density along the boundaries of packets, blocks, and laths by 1.5 times (Table 1). Such changes seem to be produced by an increase in the number of boundaries at a higher quenching temperature and a more uniform distribution of $M_{23}C_6$ carbide particles along the boundaries of blocks and laths under tempering.

In the 9–12% Cr steels containing 0.1% of carbon and 0.05% of nitrogen, special attention is paid to vanadium and niobium enriched carbonitrides MX,

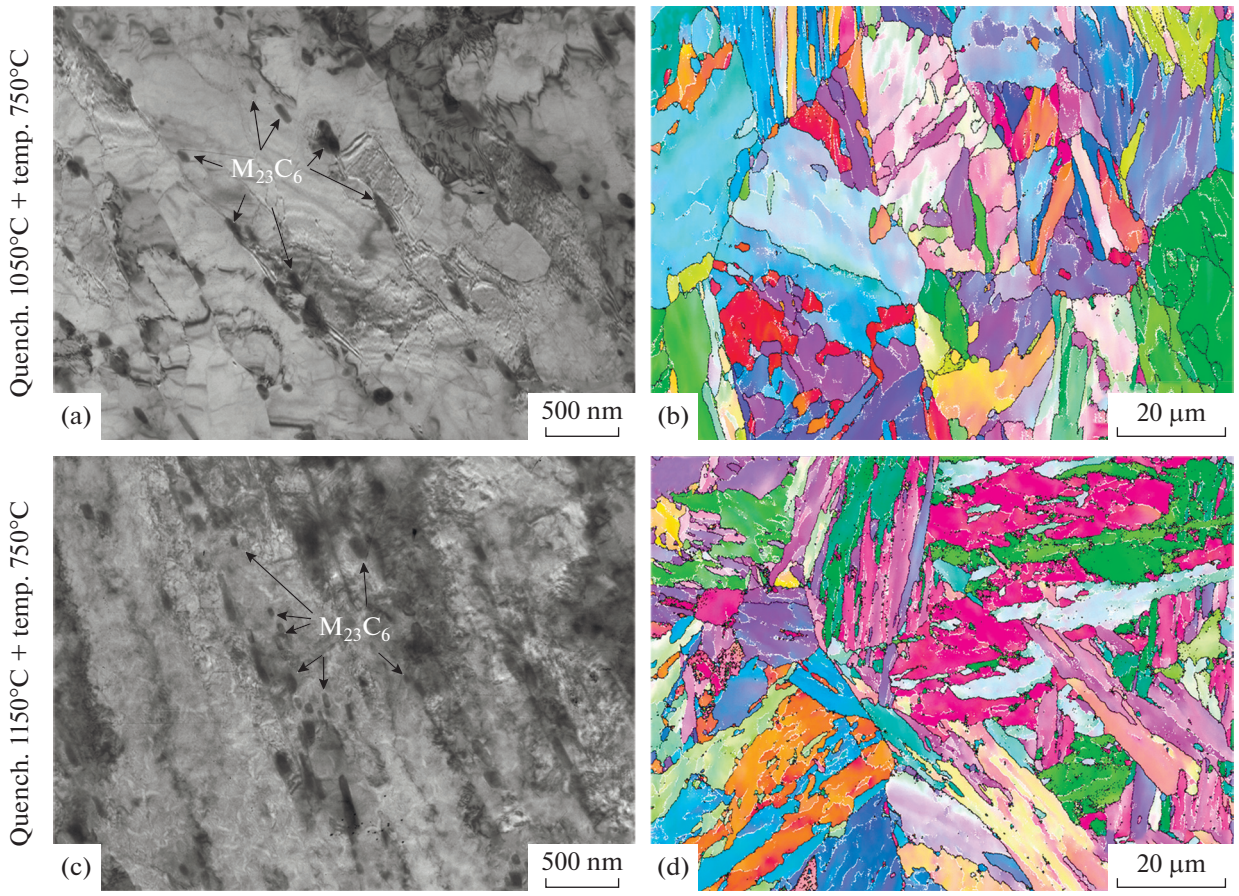

Fig. 4. Images obtained for the microstructure of steel P911 after quenching from (a), (b) 1050 and (c), (d) 1150°C with further tempering at 750°C by (a), (a) transmission electron microscopy of thin foils and (b), (d) EBSD analysis.

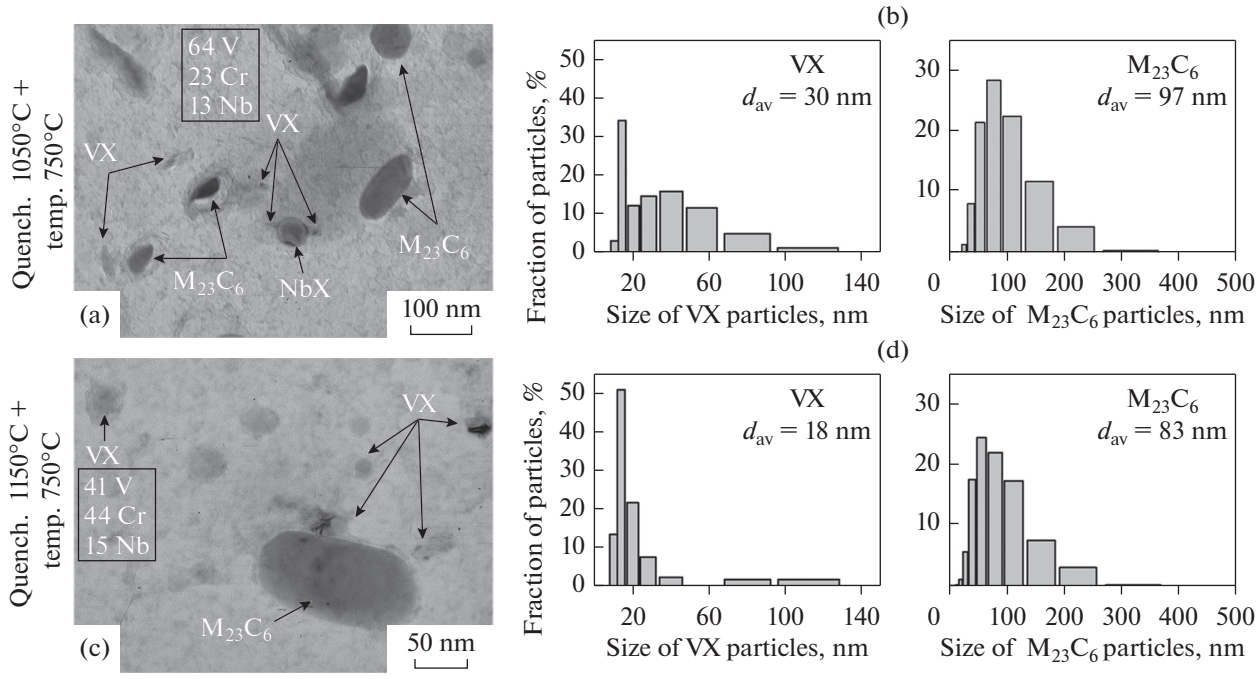

Fig. 5. (a, c) Images obtained for the particles of secondary phases in steel P911 after quenching from (a, b) 1050 and (c, d) 1150°C with further tempering at 750°C in combination with (b, d) size distribution of particles (VX and $M_{23}C_6$) by transmission electron microscopy of carbon replicas.

which are the main reasons for the appearance of threshold stresses [2, 8, 11, 17]. Different types of particles in steel P911 after quenching from 1050 and 1150°C with further tempering at 750°C are illustrated in Fig. 5 alongside their size distribution (VX and $M_{23}C_6$). In the process of tempering, the precipitation of vanadium enriched MX particles predominates independently of the quenching temperature (Fig. 5). After quenching at 1150°C, the solid solution of martensite contains an increased amount of vanadium and niobium, but this does not lead to an increase in the volume fraction of these particles (Table 1). An increase in the quenching temperature from 1050 to 1150°C leads to a two-fold decrease in the average size of VX and NbX particles under tempering (Table 1, Figs. 5b and 5d) due to an increase in the amount of MX particles precipitating in the ferrite matrix. The size distribution of VX particles (Figs. 5b and 5d) demonstrates that nearly 80% of VX particles have a size less than 25 nm after quenching from 1150°C with further tempering. The chemical composition of VX particles after quenching from 1050 and 1150°C has essential distinctions (Figs. 5a and 5c). Thus, an increase in the quenching temperature from 1050 to 1150°C changes the ratio V : Cr in VX particles from 3 : 1 to 1 : 1 (Fig. 5). Such changes in the dispersity of carbonitrides MX hinder the growth of martensite laths under tempering, thus causing their smaller size after modified heat treatment.

Hence, high creep resistance at high applied stresses in the steel with a large size of PAGs is caused by structural hardening due to a decreased size of a block and martensite laths and also by dispersion hardening predominantly due to nanosized VX particles with an average size of 18 nm. These particles hinder the climb of dislocations under creep [2, 8, 11, 17]. Let us point out that the reduction of $M_{23}C_6$ in size also must have a positive effect on the creep resistance, as these particles hinder the migration of blocks and martensite lath boundaries [15].

The elimination of increase in the creep resistance with a decrease in the applied stress is provoked by the disappearance of advantages in the structural and dispersion hardening of steel with a large size of PAGs in the process of creep. The martensite lath structure is replaced by a uniaxial subgrain structure, $M_{23}C_6$ and MX carbide particles strongly increase in size, and MX particles may be transformed into coarse stable *Z*-phase particles [1, 2, 7, 15, 17]. Such structural transformations in the process of creep must not depend on heat treatment. Further studies will be aimed at investigating the structural transformations in the process of creep.

CONCLUSIONS

The mechanical properties of steel P911 subjected to different regimes of heat treatment have been studied. An increase in the quenching temperature from

1050 to 1150°C with further tempering at 750°C leads to essential structural transformations. First, the size of PAGs grows by nearly three times to produce an effect on the size of blocks and martensite laths. The size of blocks and martensite laths is decrease by 17 and 43%, respectively. Second, the size of carbonitrides MX and carbides $M_{23}C_6$ is reduced, and the chemical composition of carbonitrides VX is changed. Such structural transformations in steel P911 produced a positive effect on the creep resistance at a temperature 650°C and applied stresses of 160, 140, and 120 MPa by increasing the time until rupture by 10, 5, and 4 times, respectively. An increase in the time until rupture under all the studied creep conditions is caused by the prolongation of the transient creep stage and a decrease in the minimum creep rate.

ACKNOWLEDGMENTS

This study was performed on the equipment of the Shared Facilities Center "Technologies and Materials" of the National Research University "Belgorod National Research University."

FUNDING

The results of studying the microstructure and mechanical properties were obtained under support from the Russian Foundation for Basic Research (grant no. 20-33-90117). The results of modeling the phase compositions were obtained under support of a grant from the President of the Russian Federation for the State Support of Young Russian Scientists—Candidates of Sciences (agreement no. 075-15-2021-336).

REFERENCES

1. F. Abe, T. U. Kern, and R. Viswanathan, *Creep-Resistant Steels* (Woodhead, Cambridge, 2008).
2. R. O. Kaibyshev, V. N. Skorobogatykh, and I. A. Shchenkova, "New martensitic steels for thermal power plant: Creep resistence," Phys. Met. Metallogr. **109**, 186–200 (2010).
3. R. Viswanathan and W. Bakker, "Materials for ultrasupercritical coal power plants – boiler materials: Part 1," J. Mater. Eng. Perform. **10**, 81–95 (2001).
4. V. M. Gundyrev, V. I. Zel'dovich, and V. M. Schastlivtsev, "Crystallographic analysis and the mechanism of martensitic transformation in iron alloys," Fiz. Met. Metalloved. **121**, 1142–1161 (2020).
5. V. S. Sagaradze, T. N. Kochetkova, N. V. Kataeva, K. A. Kozlov, V. A. Zavalishin, N. F. Vil'danova, V. S. Ageev, M. V. Leont'eva-Smirnova, and A. A. Nikitina, "Structure and creep of russian reactor steels with a bcc structure," Phys. Met. Metallogr. **118**, 494–506 (2017).
6. I. Nikitin, A. Fedoseeva, and R. Kaibyshev, "Strengthening mechanisms of creep-resistant 12% Cr–3% Co steel with low N and high B contents," J. Mater. Sci. **55**, 7530–7545 (2020).
7. A. E. Fedoseeva, I. S. Nikitin, N. R. Dudova, and R. O. Kaibyshev, "The effect of creep and long annealing conditions on the formation of the *Z*-phase particles," Phys. Met. Metallogr. **121**, 561–567 (2020).
8. F. Abe, "Precipitate design for creep strengthening of 9% Cr tempered martensitic steel for ultra-supercritical power plants," Sci. Tech. Adv. Mater. **9**, No. 013002 (2008).
9. K. Suzuki, S. Kumai, Y. Toda, H. Kushima, and K. Kimura, "Two-phase separation of primary MX Carbonitride during tempering in creep resistant 9Cr1MoVNb steel," ISIJ Int. **43**, 104312 (2003).
10. K. Maruyama, N. Sekido, and K. Yoshimi, "Changes in strengthening mechanisms in creep of 9Cr–1.8W–0.5Mo–VNb steel tested over wide ranges of creep conditions," ISIJ Int. **190**, No. 1089–1094 (2021).
11. A. Kostka, K-G. Tak, R. J. Hellmig, Y. Estrin, and G. Eggeler, "On the contribution of carbides and micrograin boundaries to the creep strength of tempered martensite ferritic steels," Acta Mater. **55**, 539–550 (2007).
12. K. Kimura, N. Ohi, K. Shimazu, T. Matsuo, R. Tanaka, and M. Kikuchi, "Effect of prior austenite grain size on high temperature creep properties of Cr–Mo–V rotor steel," Scr. Metall. **21**, 19–22 (1987).
13. A. Fedoseeva, I. Nikitin, E. Tkachev, R. Mishnev, N. Dudova, and R. Kaibyshev, "Effect of alloying on the nucleation and growth of Laves phase in the 9–10% Cr–3% Co martensitic steels during creep," Metals **11**, No. 60 (2021).
14. A. Zhilyaev, S. Sergeev, and T. Langdon, "Electron backscatter diffraction (EBSD) microstructure evolution in HPT copper annealed at a low temperature," J. Mater. Res. Technol. **3**, 338–343 (2014).
15. A. Fedoseeva, N. Dudova, and R. Kaibyshev, "Creep strength breakdown and microstructure evolution in a 3% Co modified P92 steel," Mater. Sci. Eng., A **654**, 1–12 (2016).
16. Q. Li, "Modeling the microstructure-mechanical property relationship for a 12% Cr–2W–V–Mo–Ni power plant steel," Mater. Sci. Eng., A. **361**, 385–391 (2003).
17. V. Dudko, A. Belyakov, and R. Kaibyshev, "Origin of threshold stresses in a P92-type steel," Trans. Ind. Inst. Met. **69**, 223–227 (2016).

Translated by E. Glushachenkova